Available online at http://scik.org
Commun. Math. Biol. Neurosci. 2025, 2025:54
https://doi.org/10.28919/cmbn/9234
ISSN: 2052-2541

TRANSFERRING CONTROL STRATEGIES IN EPIDEMIOLOGICAL MODELS USING τ-EQUIVALENCES

OUSSAMA CHAYOUKH*, OMAR ZAKARY

Department of Mathematics and Computer Science, Faculty of Sciences Ben M'Sik, Hassan II University of Casablanca, Commandant Driss Elharti Avenue, Casablanca 20800, Morocco

Copyright © 2025 the author(s). This is an open access article distributed under the Creative Commons Attribution License, which permits unrestricted use, distribution, and reproduction in any medium, provided the original work is properly cited.

Abstract. Mathematical modeling plays a crucial role in understanding and controlling infectious diseases. Traditional SIR models, including both demographic (incorporating births and deaths) and non-demographic variations, have been extensively used to develop control strategies. However, the transfer of control strategies derived from simpler non-demographic models to more realistic demographic models remains challenging. This research addresses this gap by exploring the concept of τ-equivalence, aiming to transfer control strategies derived from non-demographic SIR models to demographic ones. Employing numerical simulations and parameter optimization, we demonstrated that appropriately calibrated non-demographic models closely mirrored demographic model dynamics, particularly under moderate control intensities. Nevertheless, our approach faced limitations under scenarios requiring rapid and significant infection reduction, revealing potential stability challenges. Our findings highlight the practical value of the τ-equivalence calibration method, while acknowledging that its broader applicability across diverse epidemiological models warrants further investigation.

Keywords: epidemiological modeling; SIR model control; demographic dynamics; parameter calibration.

2020 AMS Subject Classification: 35A01, 65L10, 65L12, 65L20, 65L70.

*Corresponding author

E-mail address: chayoukhoussama@gmail.com

Received March 8, 2025

1. INTRODUCTION

Mathematical modeling plays a vital role in epidemiology by offering insights into the spread and control of infectious diseases [1, 2]. Among these models, the traditional Susceptible-Infected-Removed (SIR) framework, established by Kermack and McKendrick [3], is well known for its ease of use and capacity to monitor disease dynamics by examining an individual's movement between health states. Nevertheless, for chronic diseases or those requiring vital dynamics, it is essential to incorporate demographic elements [2, 4], including births and deaths, into these models to capture the impact of population changes across time as demonstrated in several studies [5, 6, 7, 8]. This results in what we refer to as demographic SIR models. Nonetheless, while this model has been extensively examined over the years, this paper employs it to demonstrate the efficacy of our method within a simplistic framework. This serves as a precursor to its application in more complex models.

Controllability is the capacity to use an acceptable control function to steer a system from any beginning state to a desired state. Since most infectious diseases require a mix of isolation, quarantine, vaccination, and treatment to be eradicated, one may refer to this as control in mathematical epidemiology [9]. Reducing the number of infected people over time or making sure the infection curve flattens within a given time period are common control goals [10, 11].

Optimal control theory has emerged as a highly effective tool for managing and mitigating a variety of diseases, with successful applications across multiple domains. It has been used extensively in the control of diseases such as tuberculosis [12, 13, 14, 15, 16], malaria [17, 18], human immunodeficiency viruses (HIV) [19, 20, 21, 22, 23, 24, 25, 26, 27], hepatitis [28, 29], and viral outbreaks such as influenza, severe acute respiratory syndromes (SARS), and coronavirus disease 2019 (COVID-19) [30, 31, 32, 33]. Its application in general SIR models has been particularly noteworthy, with several studies demonstrating how optimal control techniques can effectively guide interventions, minimizing infection rates while balancing associated costs [34, 35, 36, 37, 38]. As demonstrated in most of the previously cited literature, the Pontryagin Minimum Principle (PMP) [39] is widely employed to determine optimal control strategies that minimize intervention costs while reducing the size of the infected population [37, 40, 41, 42]. However, sometimes real-world scenarios demand not only minimizing

infections but also achieving specific outcomes—such as reducing the number of infected individuals—within a predefined timeframe that PMP does not always guarantee. This paper adopts such an approach.

In line with this objective, a control formula developed for non-demographic SIR models, as demonstrated in the work of Zakary et al. [43], provides a promising foundation by steering a basic SIR model (1), as in [3], toward a desirable infection state I_d within a given time limit T.

$$\begin{cases} \dfrac{dS}{dt} = -\dfrac{\beta}{N}SI, \\ \dfrac{dI}{dt} = \dfrac{\beta}{N}SI - \gamma I, \\ \dfrac{dR}{dt} = \gamma I, \end{cases} \tag{1}$$

where S, I, and R represent the susceptible, infected, and removed populations, respectively, β is the transmission rate, and γ is the recovery rate.

The proposed control function, denoted here as $u_z(t)$ is defined as:

$$u_z = \frac{\beta S_0}{N} Q_2^{Q_1} + Q_3 - \gamma, \tag{2}$$

where:

$$\begin{aligned} a &= \frac{I_d \exp\left((\varepsilon+\gamma)T\right) - I_0}{I_0 - I_d} \\ Q_1 &= \frac{\beta I_0 (1+a)}{aN(\varepsilon+\gamma)} \\ Q_2 &= \frac{a + \exp\left(t(\varepsilon+\gamma)\right)}{(1+a)\exp\left(t(\varepsilon+\gamma)\right)} \\ Q_3 &= \frac{(\varepsilon+\gamma)\exp\left((\varepsilon+\gamma)t\right)}{\exp\left((\varepsilon+\gamma)t\right) + a}. \end{aligned} \tag{3}$$

The control (2) employs two key parameters, ε and a, to manage infection dynamics effectively. The parameter ε ensures that the control function $u(t)$ stays within the admissible range $0 < u(t) < 1$ for all $t > 0$. For this to hold, it is sufficient for ε to satisfy the condition :

$$\gamma a - \frac{\beta S_0}{N} < \varepsilon < 1 - \frac{\beta S_0}{N} \tag{4}$$

Moreover, a is calibrated to guide the infection count toward a target threshold I_d at time T.

Nevertheless, of course, applying this strategy directly to demographic models would not be appropriate due to the lack of vital dynamics. To bridge this gap, we propose a novel adaptation: calibrating the control parameters of a non-demographic SIR model to align with those of a demographic one.

In epidemiology, epidemics might share some similarities when it comes to their dynamics [44]. As will be discussed soon, the approach we are adopting makes use of the idea of model equivalencies, where two epidemics are considered equivalent if they exhibit similar dynamics, regardless of differences in timescales.

In this paper, we specifically address the question: can a control law derived for a non-demographic SIR model, once calibrated for demographic parameters, effectively guide infection trajectories to a predetermined level *within a fixed time horizon*? We explore this for a range of ε values and desired outcomes (T, I_d).

The remainder of this paper is organized as follows: Sect. 2 presents the mathematical formulation of the demographic SIR model, including the adaptations required to apply a non-demographic control strategy. This section also introduces the calibration process and defines the concept of τ-equivalence, which ensures alignment between demographic and non-demographic models. In Sect. 3, we detail the numerical simulation results, focusing on the control function's effectiveness across different scenarios and analyzing control admissibility and delay errors. Finally, we end with Sect. 4 of conclusion.

2. METHODS

2.1. Model Formulation. We chose a similar SIR model to (1) but incorporating demographic information. It includes the following differential equations:

$$\begin{cases} \dfrac{dS}{dt} = \mu N - \dfrac{\beta}{N} SI - \mu S, \\ \dfrac{dI}{dt} = \dfrac{\beta}{N} SI - \gamma I - \mu I, \\ \dfrac{dR}{dt} = \gamma I - \mu R, \end{cases} \tag{5}$$

By adjusting the temporal unit—shifting from days to weeks or months, for instance—we can effectively align the two models.

where μ is the birth-death rate. and this is the control system:

$$\begin{cases} \dfrac{dS}{dt} = \mu N - \dfrac{\beta}{N} SI - \mu S, \\ \dfrac{dI}{dt} = \dfrac{\beta}{N} SI - (\gamma + \mu + \hat{u_z}) I, \\ \dfrac{dR}{dt} = -\mu R + (\gamma + \hat{u_z}) I, \end{cases} \tag{6}$$

2.2. Calibration and τ-Equivalence. We have to ensure that the demographic and non-demographic SIR models behave similarly over a specified time, enabling the transfer of control strategies from one model to the other with minimal deviation. To achieve this, we defined the concept of **τ-equivalence**:

Definition 1. Let (A) and (B) denote two distinct SIR model systems. For $t \in [0, t_f]$, $I_A(t), S_A(t), R_A(t)$ represent the infected, susceptible, and removed populations of system (A) at time t, while $I_B(t), S_B(t), R_B(t)$ correspond to the same populations in system (B).

(A) and (B) are considered **τ-equivalent** if their solution trajectories align closely over time within a predefined tolerance $\tau > 0$, i.e.:

$$\frac{1}{3t_f} \int_0^{t_f} \Delta_I(t)^2 + \Delta_S(t)^2 + \Delta_R(t)^2 \, dt \leq \tau^2, \tag{7}$$

where $\Delta_I(t) = |I_A(t) - I_B(t)|$, $\Delta_S(t) = |S_A(t) - S_B(t)|$, and $\Delta_R(t) = |R_A(t) - R_B(t)|$.

Here, τ represents the maximum permissible deviation between systems, which guarantees that their behaviors remain sufficiently aligned to enable effective control transfer. Small τ means the two models are effectively capturing the same epidemic outcomes from the perspective of policymakers. The inequality (7) emphasizes the importance of penalizing large discrepancies, achieved by adopting a continuous version of the Mean Squared Error (MSE) as the error metric. Moreover, by defining τ in this squared form, we align our metric with the squared differences within the continuous MSE integral, providing a logical consistency and a practical measure of error.

To determine the calibrated parameters $\hat{\beta}$ and $\hat{\gamma}$ for the non-demographic model, we seek values that satisfy the τ-equivalence condition as defined in equation (7). This is achieved by employing MATLAB$^{\text{TM}}$'s `fminsearch` function to minimize the integral within the τ-equivalence definition, ensuring it remains below the threshold of τ^2.

2.3. Control Implementation. After extracting the calibrated parameters, we substituted them into (2) to obtain the desired control function that has been implemented in the demographic SIR model. Then we used the Runge-Kutta 4th-order approach (RK4) with a step size of $h = 0.01$ to solve the controlled system. The system was then examined under four distinct scenarios, each of which represented a particular combination of the desired time T and the intended infected condition I_d. To evaluate the control's behavior and efficacy in reaching the intended infected condition within the allotted time in each epsilon value, the control was computed for each case using a range of acceptable ε values.

For each case, we focused on two aspects: the evolution of the infected population $I(t)$ and the behavior of the control function $u(t)$. We plotted the trajectories of $I(t)$ over time and evaluated how well the infected state converged to I_d. Simultaneously, we monitored the control $u(t)$ to parallel its trajectory with $I(t)$ and to ensure it remained within the admissible range $[0,1]$. These analyses allowed us to identify patterns in the system's response to different epsilon values and provided insights into the optimal control strategies for each scenario.

2.4. Delay. A delay error (8) was defined as the absolute difference between the target time T and the actual time T^* at which the controlled demographic model achieved the intended infected condition I_d at the stated time T.

$$\text{Delay} = |T - T^*|. \tag{8}$$

We computed (8) for all conceivable values of T and I_d, as well as for various values of epsilon. This highlighted critical cases where this approach may encounter limitations.

3. Numerical Simulation & Results

In this section, we detail the simulation outcomes using parameters outlined in Table 1. The time frame chosen for this study is 40 months. The tolerance threshold τ was selected iteratively to balance computational feasibility and alignment accuracy. This corresponds to an average error of approximately 1.5% of the total population (10,000 individuals), a margin deemed acceptable in epidemiological modeling where minor deviations are often tolerated to prioritize practical control strategies over perfect numerical alignment. While public health

tolerances for error may vary depending on disease severity, this threshold reflects a methodological compromise between precision and adaptability. Further sensitivity analyses could refine τ for context-specific applications.

TABLE 1. Model Parameters and Initial Conditions

Parameter	Description	Value
β	Transmission rate	0.4
γ	Recovery rate	0.01
μ	Mortality rate	0.01
S_0	Initial susceptible population	9200
I_0	Initial infected population	800
R_0	Initial removed population	0
τ	Maximum permissible deviation	150

3.1. Calibration & Equivalence. The results of calibration demonstrate a strong alignment between the demographic and calibrated non-demographic SIR models, indicating effective calibration. In Fig. 1, the susceptible, infected, and removed population graphs show near-perfect alignment between the two models for most of the 40-month interval. This is good evidence to say that the calibrated model closely mirrors the behavior of the demographic model. Small discrepancies begin to emerge beyond approximately 25 months. For the susceptible population, the calibrated model estimates slightly fewer susceptibles than the demographic model, while for the infected population, the calibrated estimates are marginally higher. The most noticeable deviation occurs in the removed population, where the calibrated model projects around 1,000 additional individuals in the later months.

Despite these small deviations, the overall alignment remains well within acceptable limits, supporting the models' τ-equivalence for our study's objectives. The calibrated parameters that achieved this alignment are $\hat{\beta} \approx 0.3781$ and $\hat{\gamma} \approx 0.0094$. The square root of the MSE for the resulting model, approximately 122.83, falls below the tolerance threshold τ, further validating

These graphs are plotted using the same RK4 approach as we explained in Section 2.3.

the equivalence. Thus, the calibrated non-demographic model provides a good approximation of the demographic SIR model, allowing us to confidently apply control strategies intended for the non-demographic model in a demographic context. However, we first need to check admissibility.

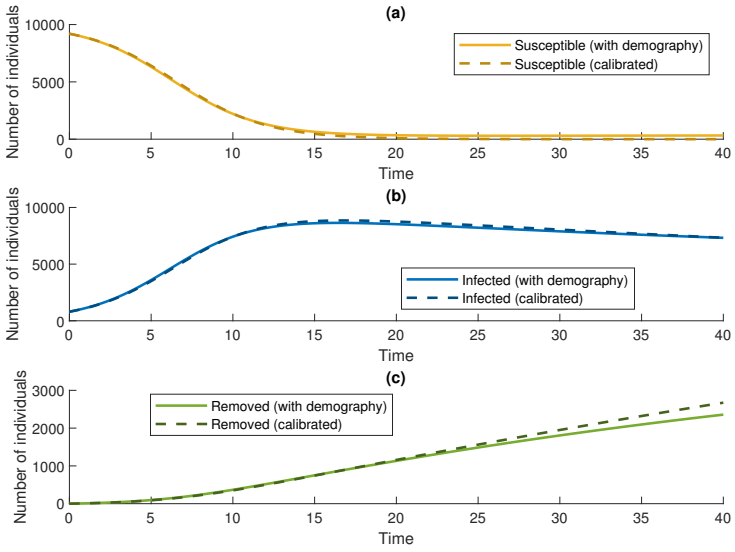

FIGURE 1. Comparison of the demographic and calibrated non-demographic SIR models over a period of 40 months. Each graph represents the population dynamics for a specific compartment: (a) susceptible population, (b) infected population, and (c) removed population

3.2. Control Dynamics and Infected States. The figures obtained from the four cases reveal the interaction between the control parameter dynamics and the infected state trajectories under varying epsilon values. Each case exhibits distinct patterns that illustrate the trade-off between speed and stability, the effects of control intensity, and how dynamic adjustments in control influence infection outcomes.

In Fig. 2, where $T = 10$ and $I_d = 100$, the infected state decreases rapidly for larger epsilon values, though the decline slows down after the desired state is reached. Smaller epsilon values, such as $\varepsilon = 0.15$ and $\varepsilon = 0.2$, result in a steady and continuous decline in control, reflecting a conservative intervention approach. As ε increases to $\varepsilon = 0.4$, the control develops an increasing pattern, stabilizing around 0.7 toward the end. For the largest epsilon values ($\varepsilon = 0.6$ and

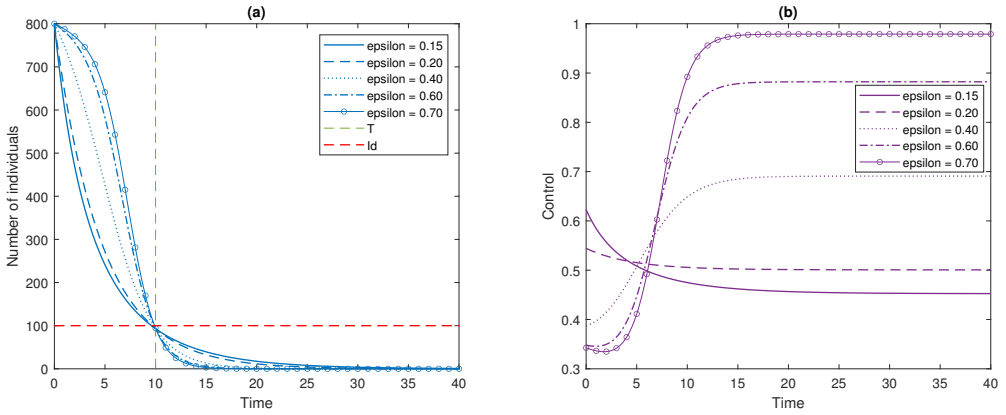

FIGURE 2. Comparison of the infected population I dynamics (a) and control values (b) over time for various epsilon values with $I_d = 100$ and $T = 10$

$\varepsilon = 0.8$), the control reaches a plateau close to 1 shortly after $t = 15$, maintaining the maximum intensity. This sustained high level of control ensures that the infected population remains low, though it also explains the slow decline observed after the desired state is achieved. This case highlights how higher epsilon values lead to faster reductions in infections but require continuous high-intensity intervention to maintain the target state.

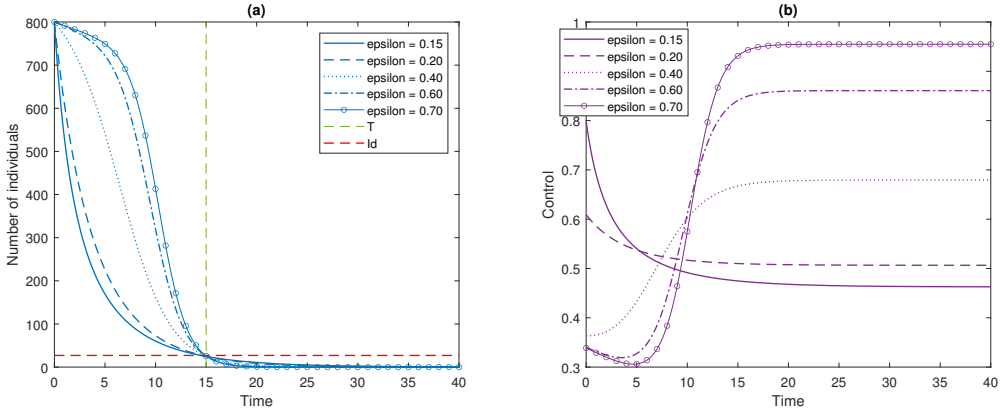

FIGURE 3. Comparison of the infected population I dynamics (a) and control values (b) over time for various epsilon values, with $I_d = 27$ and $T = 15$

As we see in Fig. 3, where $T = 15$ and $I_d = 27$, the behavior follows a similar pattern, though with smoother transitions. For smaller epsilon values ($\varepsilon = 0.15$ and $\varepsilon = 0.2$), the control steadily decreases, eventually stabilizing around 0.5. The infected state decreases smoothly throughout the time period, reflecting the stability of the control intervention. For intermediate and larger

epsilon values, such as $\varepsilon = 0.4$, $\varepsilon = 0.6$, and $\varepsilon = 0.8$, the control follows a dynamic increase-decrease-increase pattern. After an initial dip around $t = 5$, the control increases sharply and reaches a maximum plateau around $t = 15$, ensuring that the infected state remains stable once the target is achieved. The faster reductions in infections for higher epsilon values reflect the more intense control, while the dynamic adjustments in control ensure that the intervention remains effective without overshooting.

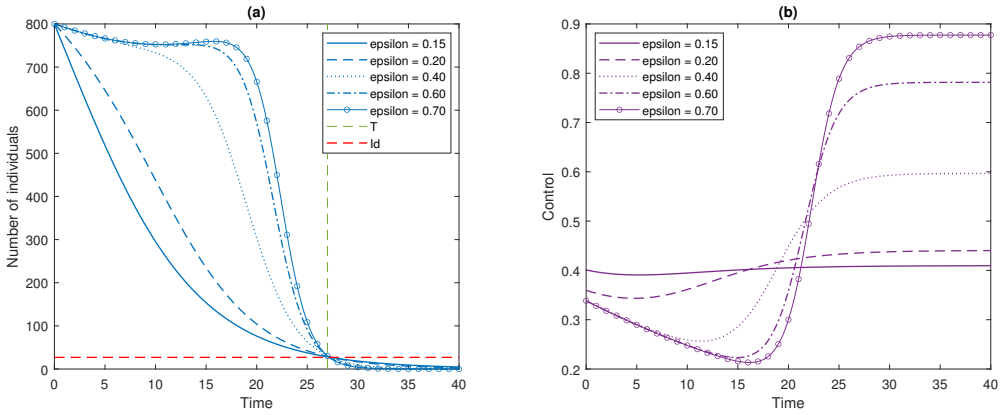

FIGURE 4. Comparison of the infected population I dynamics (a) and control values (b) over time for various epsilon values, with $I_d = 27$ and $T = 27$

However, in Fig. 4, with $T = 27$ and $I_d = 27$, the control dynamics exhibit more fluctuations, especially for higher epsilon values. For $\varepsilon = 0.15$, the control steadily decreases throughout the time interval, while $\varepsilon = 0.2$ shows an initial decrease followed by an increase, reflecting the system's adaptive response to infections. As ε increases further to $\varepsilon = 0.4$, $\varepsilon = 0.6$, and $\varepsilon = 0.8$, the control becomes more dynamic, with sharp increases occurring between $t = 15$ and $t = 20$ before stabilizing near 1. These fluctuations explain the temporary rebound in infections observed mid-way through the time period for larger epsilon values. The infected state initially decreases rapidly but experiences slight instability due to the changing control dynamics, demonstrating how larger epsilon values can introduce fluctuations even while ensuring faster convergence to the desired state.

Finally, in Fig. 5, with $T = 35$ and $I_d = 27$, the interaction between control and infected states becomes more complex. For smaller epsilon values, the control decreases steadily, maintaining a linear pattern. However, for larger epsilon values ($\varepsilon = 0.6$ and $\varepsilon = 0.8$), the infected states

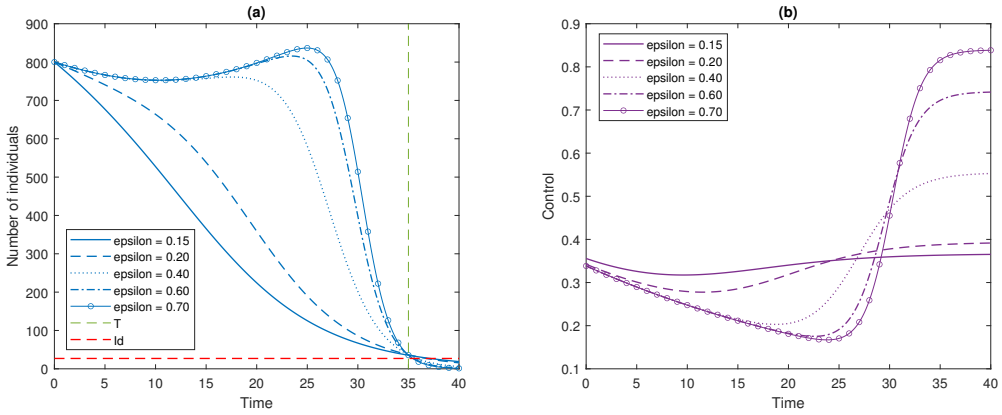

FIGURE 5. Comparison of the infected population I dynamics (a) and control values (b) over time for various epsilon values, with $I_d = 27$ and $T = 35$

exhibit a noticeable bump between $t = 20$ and $t = 30$, where infections decrease temporarily before increasing again. This behavior explains the brief resurgence in infections observed for higher epsilon values before the infected state finally stabilizes. Toward the end of the time period, the control reaches a plateau near 1, ensuring that the desired state is maintained without further fluctuations. This case demonstrates how aggressive interventions with high epsilon values can lead to temporary instabilities but are necessary for long-term stability in the infected state.

These four cases together illustrate the importance of balancing control intensity and stability when designing interventions. Higher epsilon values offer faster reductions in infections but require careful tuning to avoid instabilities and fluctuations. Smaller epsilon values ensure smoother control and more stable outcomes but may require longer time periods to achieve the desired state. Intermediate epsilon values, such as $\varepsilon = 0.4$, often strike the best balance, providing effective reductions in infections without large swings in control intensity. These insights highlight the need for dynamic and context-specific control strategies, especially in systems with varying time horizons and target states.

Although all epsilon values bring the infected population to the desired state at the desired time, the dynamics of the intervention vary significantly. For higher epsilon values, the control becomes more intense, increasing the risk of exceeding the admissible range $]0,1[$. Early in the intervention process, these values often exhibit a plateau, where infections decline slowly at

first. However, the decline becomes more aggressive as the system approaches the desired state. After reaching the target state, higher epsilon values ensure a faster reduction to zero infections, though they risk instability and inadmissibility.

In contrast, smaller epsilon values produce smoother, more uniform control. This ensures earlier recovery for some individuals, but the overall process takes longer to reach zero infections after hitting the desired state. The interventions with smaller epsilon values are more likely to stay within the admissible range, maintaining stable control without aggressive intensity.

Intermediate epsilon values, such as $\varepsilon = 0.4$, offer a more balanced approach. These values avoid extreme shifts or instability, achieving the desired state on time while keeping the control admissible and effective throughout the process. This balanced performance makes moderate epsilon values preferable in many scenarios.

It is evident that the error values are predominantly minimal and close to 0 across most cases. However, errors start to increase notably when I_d exceeds 180 and T surpasses 10. Interestingly, for $T = 40$ and $I_d = 200$, the error returns to approximately 3.

3.3. Error Behavior and Interpretation. Fig. 6 maps the alignment errors arising when transferring control strategies from the non-demographic to the demographic model across target states I_d and timeframes T. A critical finding is the emergence of the *High-State, Short-Time domain*—scenarios where aggressive targets ($I_d > 500$) under tight deadlines ($T < 20$) strain the τ-equivalence between models, leading to larger errors. Outside this domain, errors remain minimal, demonstrating the robustness of the calibration process.

The parameter ε, which governs control intensity, further modulates transfer reliability: smaller values ($\varepsilon \approx 0.1$–0.3) prioritize stability at the cost of frequent minor delays, while larger values ($\varepsilon \approx 0.7$–0.9) reduce error frequency but risk severe misalignment if the system is overdriven. This underscores the necessity of tuning ε to harmonize intensity with the fidelity of τ-equivalence—a balance critical for replicating control objectives across models.

4. CONCLUSION

In this research, we addressed the problem of transferring control strategies from non-demographic SIR models to demographic models by employing the concept of τ-equivalence. Our primary

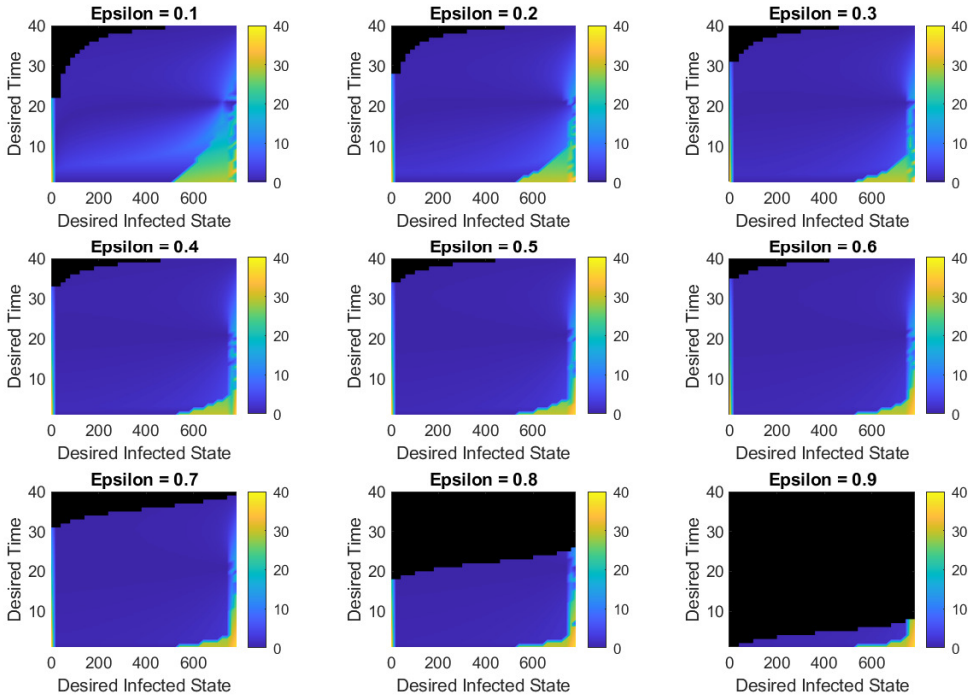

FIGURE 6. Error values calculated for every combination of desired time T (range: 0-40 months) and desired infected state I_d (range: 0 to $I_0 = 800$). The color bar spans error values from 0 months (blue) to 40 months (yellow). Errors are computed for nine cases of $\varepsilon \in \{0.1, 0.2, 0.3, 0.4, 0.5, 0.6, 0.7, 0.8, 0.9\}$. Black regions indicate inadmissible control cases where solutions are not achievable

goal was to demonstrate that, with appropriate calibration, simple non-demographic models can effectively guide infection control in more complex demographic scenarios involving births and deaths.

Our findings confirmed that calibrated non-demographic models can reliably replicate demographic model dynamics within acceptable error margins, validating the effectiveness of the τ-equivalence approach. We observed that moderate control intensities (intermediate ε values) provided optimal performance by achieving a balance between timely infection control and stability. Conversely, extreme ε values posed challenges, either causing overly aggressive interventions or overly cautious responses.

A key limitation of this study is the diminished performance observed under highly demanding conditions—specifically scenarios requiring rapid, substantial infection reduction—highlighting potential challenges in real-world applications where aggressive intervention timelines might be necessary. Additionally, our method was tested exclusively on a relatively simple model (the SIR model). Although successful in this context, the applicability of τ-equivalence for transferring control strategies between more complex or fundamentally different epidemiological models remains an open question.

The results emphasize the practical implications of calibrating simpler models for controlling complex epidemiological dynamics. Future research may address the identified limitations by integrating additional factors such as spatial heterogeneity, age structure, or seasonal effects. Exploring multi-objective optimization frameworks and testing τ-equivalence across different classes of epidemiological models could further enhance the flexibility and practical effectiveness of these control strategies.

CONFLICT OF INTERESTS

The authors declare that there is no conflict of interests.

REFERENCES

[1] F. Brauer, C. Castillo-Chavez, Mathematical Models in Population Biology and Epidemiology, Springer New York, 2012. https://doi.org/10.1007/978-1-4614-1686-9.

[2] F. Brauer, P. Van Den Driessche, J. Wu, eds., Mathematical Epidemiology, Springer, Berlin, 2008. https://doi.org/10.1007/978-3-540-78911-6.

[3] W.O. Kermack, A.G. McKendrick, A Contribution to the Mathematical Theory of Epidemics, Proc. R. Soc. London. Ser. A 115 (1927), 700–721. https://doi.org/10.1098/rspa.1927.0118.

[4] S.N. Busenberg, K.P. Hadeler, Demography and Epidemics, Math. Biosci. 101 (1990), 63–74. https://doi.org/10.1016/0025-5564(90)90102-5.

[5] S. Busenberg, P. Van Den Driessche, Analysis of a Disease Transmission Model in a Population with Varying Size, J. Math. Biol. 28 (1990), 257–270. https://doi.org/10.1007/BF00178776.

[6] W.R. Derrick, P. Van Den Driessche, A Disease Transmission Model in a Nonconstant Population, J. Math. Biol. 31 (1993), 495–512. https://doi.org/10.1007/BF00173889.

[7] M. Martcheva, C. Castillo-Chavez, Diseases with Chronic Stage in a Population with Varying Size, Math. Biosci. 182 (2003), 1–25. https://doi.org/10.1016/S0025-5564(02)00184-0.

[8] R.M. Anderson, R.M. May, Infectious Diseases of Humans: Dynamics and Control, Oxford University Press, Oxford, 1991. https://doi.org/10.1093/oso/9780198545996.001.0001.

[9] O. Sharomi, T. Malik, Optimal Control in Epidemiology, Ann. Oper. Res. 251 (2017), 55–71. https://doi.org/10.1007/s10479-015-1834-4.

[10] J. Klamka, Controllability of Dynamical Systems. A Survey, Bull. Pol. Acad. Sci.: Tech. Sci. 61 (2013), 335–342. https://doi.org/10.2478/bpasts-2013-0031.

[11] H.J. Sussmann, V. Jurdjevic, Controllability of Nonlinear Systems, J. Differ. Equ. 12 (1972), 95–116. https://doi.org/10.1016/0022-0396(72)90007-1.

[12] E. Jung, S. Lenhart, Z. Feng, Optimal Control of Treatments in a Two-Strain Tuberculosis Model, Discrete Contin. Dyn. Syst. B 2 (2002), 473–482. https://doi.org/10.3934/dcdsb.2002.2.473.

[13] D.P. Moualeu, M. Weiser, R. Ehrig, P. Deuflhard, Optimal Control for a Tuberculosis Model with Undetected Cases in Cameroon, Commun. Nonlinear Sci. Numer. Simul. 20 (2015), 986–1003. https://doi.org/10.1016/j.cnsns.2014.06.037.

[14] C.J. Silva, D.F.M. Torres, Optimal Control for a Tuberculosis Model with Reinfection and Post-Exposure Interventions, Math. Biosci. 244 (2013), 154–164. https://doi.org/10.1016/j.mbs.2013.05.005.

[15] F.B. Agusto, A.I. Adekunle, Optimal Control of a Two-Strain Tuberculosis-HIV/AIDS Co-Infection Model, Biosystems 119 (2014), 20–44. https://doi.org/10.1016/j.biosystems.2014.03.006.

[16] S. Whang, S. Choi, E. Jung, A Dynamic Model for Tuberculosis Transmission and Optimal Treatment Strategies in South Korea, J. Theor. Biol. 279 (2011), 120–131. https://doi.org/10.1016/j.jtbi.2011.03.009.

[17] B.N. Kim, K. Nah, C. Chu, S.U. Ryu, Y.H. Kang, Y. Kim, Optimal Control Strategy of Plasmodium Vivax Malaria Transmission in Korea, Osong Public Health Res. Perspect. 3 (2012), 128–136. https://doi.org/10.1016/j.phrp.2012.07.005.

[18] O. Prosper, N. Ruktanonchai, M. Martcheva, Optimal Vaccination and Bednet Maintenance for the Control of Malaria in a Region with Naturally Acquired Immunity, J. Theor. Biol. 353 (2014), 142–156. https://doi.org/10.1016/j.jtbi.2014.03.013.

[19] H.R. Joshi, Optimal Control of an HIV Immunology Model, Optim. Control Appl. Methods 23 (2002), 199–213. https://doi.org/10.1002/oca.710.

[20] K.R. Fister, S. Lenhart, J.S. McNally, Optimizing Chemotherapy in an HIV Model, Electron. J. Differ. Equ. 1998 (1998), 32.

[21] Y. Yang, Y. Xiao, J. Wu, Pulse HIV Vaccination: Feasibility for Virus Eradication and Optimal Vaccination Schedule, Bull. Math. Biol. 75 (2013), 725–751. https://doi.org/10.1007/s11538-013-9831-8.

[22] H.D. Kwon, J. Lee, S.D. Yang, Optimal Control of an Age-Structured Model of HIV Infection, Appl. Math. Comput. 219 (2012), 2766–2779. https://doi.org/10.1016/j.amc.2012.09.003.

[23] M. Roshanfekr, M.H. Farahi, R. Rahbarian, A Different Approach of Optimal Control on an HIV Immunology Model, Ain Shams Eng. J. 5 (2014), 213–219. https://doi.org/10.1016/j.asej.2013.05.004.

[24] Y. Zhou, Y. Liang, J. Wu, An Optimal Strategy for HIV Multitherapy, J. Comput. Appl. Math. 263 (2014), 326–337. https://doi.org/10.1016/j.cam.2013.12.007.

[25] B.M. Adams, H.T. Banks, M. Davidian, H.-D. Kwon, H.T. Tran, S.N. Wynne, E.S. Rosenberg, HIV Dynamics: Modeling, Data Analysis, and Optimal Treatment Protocols, J. Comput. Appl. Math. 184 (2005), 10–49. https://doi.org/10.1016/j.cam.2005.02.004.

[26] V. Costanza, P.S. Rivadeneira, F.L. Biafore, C.E. D'Attellis, Optimizing Thymic Recovery in HIV Patients through Multidrug Therapies, Biomed. Signal Process. Control 8 (2013), 90–97. https://doi.org/10.1016/j.bspc.2012.06.002.

[27] O. Zakary, M. Rachik, I. Elmouki, On the Impact of Awareness Programs in HIV/AIDS Prevention: An SIR Model with Optimal Control, Int. J. Comput. Appl. 133 (2016), 1–6. https://doi.org/10.5120/ijca2016908030.

[28] L. Rong, A.S. Perelson, Treatment of Hepatitis C Virus Infection With Interferon and Small Molecule Direct Antivirals: Viral Kinetics and Modeling, Crit. Rev. Immunol. 30 (2010), 131–148. https://doi.org/10.1615/CritRevImmunol.v30.i2.30.

[29] O. Zakary, M. Rachik, I. Elmouki, On Effectiveness of an Optimal Antiviral Bitherapy in HBV-HDV Coinfection Model, Int. J. Comput. Appl. 127 (2015), 1–10. https://doi.org/10.5120/ijca2015906554.

[30] F.B. Agusto, Optimal Isolation Control Strategies and Cost-Effectiveness Analysis of a Two-Strain Avian Influenza Model, Biosystems 113 (2013), 155–164. https://doi.org/10.1016/j.biosystems.2013.06.004.

[31] X. Yan, Y. Zou, Optimal and Sub-Optimal Quarantine and Isolation Control in SARS Epidemics, Math. Comput. Model. 47 (2008), 235–245. https://doi.org/10.1016/j.mcm.2007.04.003.

[32] Y. Li, Optimal Control for an Epidemic Model of COVID-19 with Time-Varying Parameters, Mathematics 12 (2024), 1484. https://doi.org/10.3390/math12101484.

[33] S. Seddighi Chaharborj, S. Seddighi Chaharborj, J. Hassanzadeh Asl, P.S. Phang, Controlling of Pandemic COVID-19 Using Optimal Control Theory, Results Phys. 26 (2021), 104311. https://doi.org/10.1016/j.rinp.2021.104311.

[34] M. Elhia, M. Rachik, E. Benlahmar, Optimal Control of an SIR Model with Delay in State and Control Variables, ISRN Biomath. 2013 (2013), 403549. https://doi.org/10.1155/2013/403549.

[35] A. El-Alami Laaroussi, M. Rachik, M. Elhia, An Optimal Control Problem for a Spatiotemporal SIR Model, Int. J. Dyn. Control 6 (2018), 384–397. https://doi.org/10.1007/s40435-016-0283-5.

[36] L. Bolzoni, R. Della Marca, M. Groppi, On the Optimal Control of SIR Model with Erlang-Distributed Infectious Period: Isolation Strategies, J. Math. Biol. 83 (2021), 36. https://doi.org/10.1007/s00285-021-01668-1.

[37] O. Zakary, M. Rachik, I. Elmouki, On the Analysis of a Multi-Regions Discrete SIR Epidemic Model: An Optimal Control Approach, Int. J. Dyn. Control 5 (2017), 917–930. https://doi.org/10.1007/s40435-016-0233-2.

[38] O. Zakary, M. Rachik, I. Elmouki, A New Analysis of Infection Dynamics: Multi-Regions Discrete Epidemic Model with an Extended Optimal Control Approach, Int. J. Dyn. Control 5 (2017), 1010–1019. https://doi.org/10.1007/s40435-016-0264-8.

[39] L.S. Pontryagin, Mathematical Theory of Optimal Processes, CRC Press, 1987.

[40] L. Bolzoni, E. Bonacini, C. Soresina, M. Groppi, Time-Optimal Control Strategies in SIR Epidemic Models, Math. Biosci. 292 (2017), 86–96. https://doi.org/10.1016/j.mbs.2017.07.011.

[41] E.V. Grigorieva, E.N. Khailov, A. Korobeinikov, Optimal Control for a SIR Epidemic Model with Nonlinear Incidence Rate, Math. Model. Nat. Phenomena 11 (2016), 89–104. https://doi.org/10.1051/mmnp/201611407.

[42] E.A. Bakare, A. Nwagwo, E. Danso-Addo, Optimal Control Analysis of an SIR Epidemic Model with Constant Recruitment, Int. J. Appl. Math. Res. 3 (2014), 273–285. https://doi.org/10.14419/ijamr.v3i3.2872.

[43] O. Zakary, S. Bidah, M. Rachik, Optimizing Infection Trajectories: Innovation in Controllability of Nonlinear SIR Model, Rev. Mex. Ing. Bioméd. 45 (2024), 151–171. https://doi.org/10.17488/RMIB.45.2.9.

[44] T.A. Dallas, G. Foster, R.L. Richards, B.D. Elderd, Epidemic Time Series Similarity Is Related to Geographic Distance and Age Structure, Infect. Dis. Model. 7 (2022), 690–697. https://doi.org/10.1016/j.idm.2022.09.002.